

Article

The Adhesive Properties of Coherent and Semicoherent NiAl/V Interfaces Within the Peierls-Nabarro Model

Yaoyao Linghu ¹, Xiaozhi Wu ^{1,2,*}, Rui Wang ¹, Weiguo Li ³ and Qing Liu ²

¹ Institute for Structure and Function, Chongqing University, Chongqing 401331, China; 20142702010@cqu.edu.cn (Y.L.); rcwang@cqu.edu.cn (R.W.)

² College of Materials Science and Engineering, Chongqing University, Chongqing 400044, China; qingliu@cqu.edu.cn

³ College of Aerospace Engineering, Chongqing University, Chongqing 400044, China; wgli@cqu.edu.cn

* Correspondence: xiaozhiwu@cqu.edu.cn; Tel.: +86-23-6567-8367

Academic Editor: Ronald W. Armstrong

Received: 22 January 2016; Accepted: 22 March 2016; Published: 25 March 2016

Abstract: The work of adhesion and the interface energy of NiAl/V coherent interface systems have been investigated using first-principles methods. The adhesion of the Ni-terminated interface is larger than the Al-terminated interface. The difference in charge density and the density of states show that the Ni-terminated interface is dominated by metallic bonds, and the Al-terminated interface is dominated by metallic and covalent bonds. To account for the effects of misfit dislocations on the semicoherent interfaces, the Peierls–Nabarro model combined with generalized stacking fault energy is employed to determine the interface energy. It is found that misfit dislocations can reduce the adhesion of the interface, and the reduction increases with the maximum of the restoring force.

Keywords: NiAl/V; adhesion; Peierls–Nabarro model; first-principles

1. Introduction

Nickel aluminum (NiAl) is a promising material for high temperature structure materials, especially applied in the aerospace industry, due to its superior properties, including high melting temperature, high temperature strength, low density and good oxidation resistance [1–5]. However, NiAl has brittleness at room temperature and poor creep resistance at high temperature, which limit its wide application [6]. Alloying refractory metals (Cr, Mo, Re, V, W) [7–12] and the intermetallic phase of the Heusler or Laves type (Hf, Nb, Ta) [13–16] with NiAl have been verified to be feasible to achieve the improved properties of NiAl through Directional Solidification (DS); because eutectic DS is not merely single-phase intermetallics, which combine several materials with complimentary properties to perfect the original properties. For NiAl-V systems, it is reported that the fracture toughness ($32 \text{ MPa}\sqrt{m}$) of eutectic NiAl-V was the highest of all NiAl-based eutectic systems [7]. Recently, Milenkovic and Caram [17] studied the mechanical properties of NiAl-V eutectic alloy and founded that eutectic NiAl-V retains a yield strength up to 1073 K higher than NiAl and most of the NiAl-based eutectic systems, and the fracture toughness ($28.5 \text{ MPa}\sqrt{m}$) is the highest among other NiAl-based eutectic systems. The interfacial structure and adhesion between NiAl and V phases have significant influence on the composite's performances. Therefore, it is necessary to investigate the interfacial properties of NiAl-V systems. However, there is only a limited number of theoretical studies on NiAl-V interfaces.

As we know, there exists a discrepancy of the lattice constants between NiAl and V. The misfit will introduce strain and a periodic array of dislocations at the interface, and thus, the interface becomes semicoherent. Therefore, it is indispensable to analyze the misfit dislocations at the interface. The semicoherent interfaces have been investigated by some researchers using first-principles methods [18–21]. Unfortunately, the required unit cells are commonly beyond the capacity of our computer due to the long-periodicity of the dislocations. Generally, the coherent interface approximation [22] is applied to study the interfaces in which the misfit dislocation is ignored. The coherent interfaces have been investigated by many researchers [23–31]; whereas, the obtained theoretical work of adhesion is larger than the observed values [32].

An alternative method to address this problem is based on the Peierls–Nabarro (PN) framework. The original PN model describes the motion of the dislocation core through the sinusoidal potential function; whereas, the local relaxation of atoms is neglected due to the one-dimensional constraint path approximation. The modification of the original PN model has been proposed by many researchers in which the nonlinear displacement field is considered [33–36]. Here, the misfit energy is solved by combining the first-principle calculations with the isotropic continuum theory accounting for the elasticity of the materials. The model has been applied to such interfaces as Al/MgO [37,38], Fe/VN [39,40] and NiAl/Mo [41], proven to describe the interfaces properly.

In this paper, we have investigated the coherent and semicoherent interface energy. The work of adhesion and the interface energy of coherent NiAl/V interfaces have been calculated using the first-principles methods. The difference in the charge density and the states of density (DOS) have been used to analyze the interfacial bonding. In order to determine the adhesive properties of semicoherent NiAl/V interfaces, the misfit dislocations and interface energy have been investigated within the framework of the PN theory. The effects of misfit dislocations on the adhesive properties of interfaces have been also discussed.

2. Details of the Calculations

The first-principles calculations were employed with the Vienna *ab initio* Simulation Package (VASP) code developed at the Institut für Theoretische Physik of Universität Wien [42,43]. The all-electron Projector Augmented Wave (PAW) method [44,45] within Generalized Gradient Approximation (GGA) was utilized. The GGA was adopted for the exchange-correlation functional according to the Perdew–Burke–Ernzerhof (PBE) method [46]. In our paper, the self-consistent convergence was set to 10^{-5} eV/atom. Before the calculation, the convergency of the total energies with respect to k-point sampling grids obtained by the Monkhorst–Park method, and the cutoff energy was checked. The plane wave cutoff energy was fixed to 550 eV in all calculations. As for the Brillouin zone k-point grids, we used a $25 \times 25 \times 25$ k-point mesh for the bulk. The surface and interface systems were established by periodic supercell slabs containing a finite atomic slab and a vacuum layer. The thickness of the vacuum layer (15 Å) was sufficient to prevent systems from periodic images based on the convergence test. In this case, a $25 \times 25 \times 1$ k-point mesh was employed. The accuracy of our approach was guaranteed by the good agreement between the calculated data and previous results (see Table 1).

Table 1. Summary of the lattice constants a , elastic constants C_{11} , C_{12} , C_{44} , shear modulus G , bulk modulus B , Young's modulus E and Poisson's ratio ν for NiAl and V.

Materials	a (Å)	C_{11} (GPa)	C_{12} (GPa)	C_{44} (GPa)	G (GPa)	B (GPa)	E (GPa)	ν
NiAl	2.89	205.1	136.1	116.9	83.9	159.1	214.2	0.40
[47]	2.89	203	140	113	80.4	161.0	206.8	0.41
[48]	2.89	233	121	114	85	159	218	0.34
V	3.01	253.7	134.7	19.9	35.7	174.3	100.4	0.35
[49]	3.04	228.0	118.8	42.6	47.4	155.2	129.0	0.34
[50]	–	228	119	42.6	47.4	155.3	129.0	0.34

3. Bulk Properties

The optimized lattice parameters are listed in Table 1. The lattice parameters are 2.89 Å for NiAl and 3.04 Å for V, which are in good agreement with previous studies [47–50]. Elastic constants are a basic mechanical quantity describing the stiffness of the material when strains are applied. It is essential to investigate the elastic constants to know the mechanical properties of both materials. The calculated elastic constants are shown in Table 1, and they all satisfy Born's mechanical stability condition [51]. The calculated elastic constants of NiAl are well consistent with the previous values [47,48]; whereas, the obtained elastic constants for V exhibit some differences with the reported experiment values, which may due to the variation of temperature.

The bulk modulus B and shear modulus G can be obtained from the elastic constants according to the Voigt–Reuss–Hill (VRH) approximations [52]. The obtained elastic moduli listed in Table 1 are well consistent with the previous results. Young's modulus E and Poisson's ratio ν can be obtained using the bulk and shear modulus. Young's modulus characterize the stiffness of the material. The higher the value of E is, the stiffer the material is. As listed in Table 1, the obtained Young's modulus of NiAl is larger than V, which demonstrates that NiAl is stiffer than V. Poisson's ratio is associated with the material's volume change. According to Ravindran *et al.* [53], a value of σ lower than 0.5 means the volume change is related to elastic deformation. The calculated σ is separately 0.4 and 0.35 for NiAl and V, which indicates that the volume change of NiAl and V may be related to the deformation.

4. Surface Properties

To investigate the interface, it is necessary to make sure that the two slabs are thick enough to represent the bulk-like interiors. Therefore, we conducted convergence tests on NiAl (001) and V (001) slabs. To acquire the suitable thickness necessary for bulk-like NiAl and V slabs, the dependence of layer relaxation on the atom layers has been explored. In Table 2, we display the relaxed atomic arrangements of seven-layer NiAl, AlNi and V for surface energy calculations to show the surface effect intuitively. The results of interlayer relaxation Δ_{ij} (interlayer relaxation as the percentage of bulk interlayer relaxation) are displayed in Table 3, which suggest that the interface relaxations exhibited for all slabs are very large and that the surface effect is mainly restricted to the first three layers. As can be seen, the five-layer V (001) is thick enough to exhibit a bulk-like interior. As for NiAl (001), the results show that for more than seven layers, the interlayer relaxation for both terminations is well converged. Therefore, the V part with six atomic layers and the NiAl (AlNi) slab with eight atomic layers adopted in the following calculations are suitable. It is also revealed that the contraction of the top layer of the Ni-terminated surface ($\Delta_{12} = -10.9\%$) is larger than the Al-terminated surface ($\Delta_{12} = -7.0\%$), which implies that the Al-terminated slab is stabler. We calculated the surface energy of V (001) with respect to slab thickness using [54,55]:

$$\gamma_s = \frac{E_{slab} - N_{slab}E_{bulk}}{2A_s} \quad (1)$$

where E_{slab} and N_{slab} are respectively the total energy and the atom number in the slab, E_{bulk} is the energy per atom in the bulk materials and A_s is the corresponding surface area of the unit cell. The factor of two accounts for the two identical surfaces of the slab. For the V (001) surface, the calculated dependence of surface energy on the atom layers is listed in Table 4. It shows that the γ_s of V converges to 2.36 J/m², in agreement with the experimental value (2494.87 ergs cm⁻²) [56].

Table 2. The relaxed atomic arrangements of 7-layer NiAl, AlNi and V for surface energy calculations. We only show the atomic arrangements of the top four layers due to the symmetry of the supercell. The atomic position is given with respect to the basis vector of the supercell for surface calculations (Al_n, Al atoms of the n-th layer; Ni_n, Ni atoms of the n-th layer; V_n, V atoms of the n-th layer).

Systems	Symbol	Atomic Position		
		x	y	z
NiAl (Al-terminated)	Al1	0.0000	0.0000	0.0018
	Ni1	0.5000	0.5000	0.0743
	Al2	0.0000	0.0000	0.1536
	Ni2	0.5000	0.5000	0.2308
AlNi (Ni-terminated)	Ni1	0.0000	0.0000	0.0042
	Al1	0.5000	0.5000	0.0730
	Ni2	0.0000	0.0000	0.1548
	Al2	0.5000	0.5000	0.2308
V	V1	0.0000	0.0000	0.0108
	V2	0.5000	0.5000	0.0770
	V3	0.0000	0.0000	0.1539
	V4	0.5000	0.5000	0.2308

Table 3. The interlayer relaxation change (Δ_{ij}) convergence of NiAl (001), AlNi (001) and V (001) with respect to the atom layers.

Systems	Interlayer	Atom Layers of Slab				
		3	5	7	9	11
NiAl (Al terminated)	Δ_{12}	-1.4%	-6.6%	-5.7%	-6.4%	-7.0%
	Δ_{23}	-	4.2%	3.1%	3.6%	4.1%
	Δ_{34}	-	-	0.3%	1.1%	1.0%
	Δ_{45}	-	-	-	-1.3%	-0.5%
	Δ_{56}	-	-	-	-	-0.3%
AlNi (Ni terminated)	Δ_{12}	-5.3%	-10.0%	-10.7%	-10.3%	-10.9%
	Δ_{23}	-	4.8%	6.3%	7.0%	6.1%
	Δ_{34}	-	-	-1.2%	-2.8%	-1.9%
	Δ_{45}	-	-	-	0.7%	1.2%
	Δ_{56}	-	-	-	-	0.0%
V	Δ_{12}	-13.6%	-15.2%	-13.9%	-14.2%	-14.3%
	Δ_{23}	-	0.7%	0.2%	-0.7%	-0.2%
	Δ_{34}	-	-	0.3%	1.9%	2.0%
	Δ_{45}	-	-	-	-1.8%	-3.0%
	Δ_{56}	-	-	-	-	0.7%

Table 4. Convergence of the surface energy γ_s (J/m²) of NiAl (Al-terminated), AlNi (Ni-terminated) and V with respect to the number of atom layers.

Number of Layers; n	$\gamma_{s,NiAl}$		$\gamma_{s,AlNi}$		$\gamma_{s,V}$
	Stoichiometric	Non-Stoichiometric	Stoichiometric	Non-Stoichiometric	
3	–	2.63 ~ 3.96	–	3.33 ~ 4.67	–
4	2.27	–	2.27	–	2.61
5	–	2.70 ~ 4.03	–	3.27 ~ 4.60	–
6	2.31	–	2.31	–	2.36
7	–	2.69 ~ 4.03	–	3.25 ~ 4.58	–
8	2.30	–	2.30	–	2.36
9	–	2.69 ~ 4.03	–	3.25 ~ 4.58	–
10	2.30	–	2.30	–	2.36
11	–	2.69 ~ 4.03	–	3.25 ~ 4.58	–

As for the NiAl (001) surface, the situation is more complicated. The (001) surface of NiAl is distinguished by its terminated surface layer consisting of a Ni layer or a Al layer. Thus, its surface energy, which is calculated by using Equation (1), is the average value of the two terminations, and we could not obtain the surface energy for Ni-terminated or Al-terminated. What is more, the asymmetric slab will induce the spurious dipole effect [57]. The slabs using odd numbers of layers are non-stoichiometric slabs; the chemical potentials of the Ni and Al atoms should be taken into consideration when calculating the surface energies of NiAl (001) surfaces. The surface energy of Al-terminated (001) γ_s can be calculated as [58,59]:

$$\gamma_s = \frac{1}{2A_s} [E_{slab} - n_{Al}\mu_{NiAl}^{bulk} + (n_{Al} - n_{Ni})\mu_{Ni}^{slab}] \quad (2)$$

where n_{Al} , n_{Ni} are the Al and Ni atom numbers in the slab, μ_{NiAl}^{bulk} is the chemical potential per formula in bulk NiAl and μ_{Ni}^{slab} is the chemical potential of the Ni atom in the surface supercell. Assuming that the NiAl (001) surface is in equilibrium with bulk NiAl, thus, $\mu_{NiAl}^{bulk} = \mu_{Ni}^{slab} + \mu_{Al}^{slab}$. In thermodynamics, the chemical potential of NiAl in bulk, bulk NiAl formation heat (ΔH_f^0) and chemical potentials of elementary bulk Ni and Al are related by $\mu_{NiAl}^{bulk} = \mu_{Ni}^{bulk} + \mu_{Al}^{bulk} + \Delta H_f^0$. Additionally, NiAl is more stable than both elementary phases; the μ_{Al}^{slab} and μ_{Ni}^{slab} must be less than the μ_{Al}^{bulk} and μ_{Ni}^{bulk} , respectively. Combining the above relationships, we can obtain the following inequality:

$$\Delta H_f^0 \leq \mu_{Ni}^{slab} - \mu_{Ni}^{bulk} \leq 0 \quad (3)$$

where $\mu_{Ni}^{bulk} = E_{Ni}^{bulk}$ and $\mu_{Al}^{bulk} = E_{Al}^{bulk}$ are calculated on the bulk fcc-Ni and fcc-Al. The ΔH_f^0 can also be expressed by:

$$\Delta H_f^0 = E_{NiAl}^{bulk} - E_{Ni}^{bulk} - E_{Al}^{bulk} \quad (4)$$

The calculated ΔH_f^0 is -1.13 eV, and the calculated surface energies of Al- and Ni-terminated NiAl (001) based on the above equations are in the ranges of 2.69–4.03 J/m² and 3.25–4.58 J/m², respectively. This means that the Al-terminated surfaces of NiAl are more stable, which agrees well with Brown's analysis using Monte Carlo modeling [60]. The Ni-terminated surface with a larger surface energy is a reactive surface and leads to larger interfacial adhesion (see the following section). The surface energy of NiAl with even layers was also calculated by using Equation (1). The obtained γ_s of NiAl converges to 2.30 J/m² and agrees well with the previous study [54].

5. Coherent Interfaces

5.1. Interface Geometry

Our geometry of the NiAl/V interface was established by a supercell enclosing a sequence of eight NiAl and six V (001) layers stacked in the $\langle 001 \rangle$ direction. Since there is a nearly 4% lattice mismatch between the smaller NiAl unit cell and that of the V, we strain the softer V to be lattice matched (coherent interface approximation) [22] to accommodate the periodic boundary conditions on slab calculations. In reality, the mismatch will introduce an array of misfit dislocations, which will be discussed in the following section. Both NiAlV (Al-terminated) and AlNiV (Ni-terminated) interfaces were taken into account to decide which bonding was preferable. The models of the slabs are sketched in Figure 1.

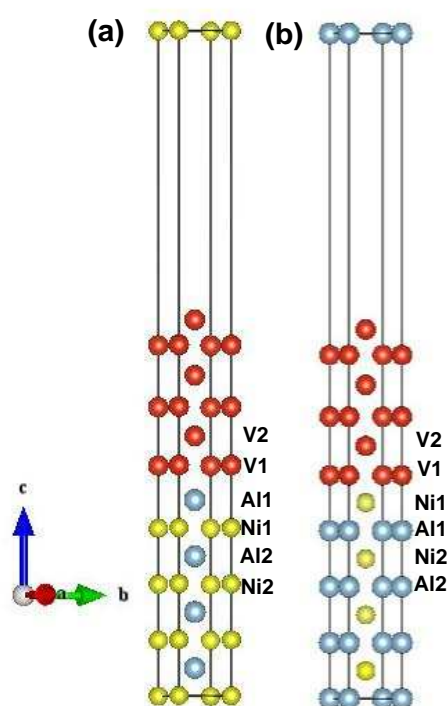


Figure 1. The supercell models for the (a) NiAlV and (b) AlNiV interfaces.

5.2. Work of Adhesion

There are two fundamental quantities widely used to describe the mechanical and thermodynamic properties of the interface. One is the ideal work of adhesion W_{ad} defined as the bond energy (per unit area) to separate an interface into two free surfaces [61]. For simplification, the plastic deformation and diffusion are neglected. Commonly, W_{ad} can be given by the difference in total energy between the interface and its isolated surfaces:

$$W_{ad} = \frac{E_{slabA} + E_{slabB} - E_{A/B}}{S} \quad (5)$$

E_{slab} is the total energy of isolated NiAl or V slabs in the same supercell; $E_{A/B}$ is the energy of the interface systems; and S is the corresponding interface area.

The W_{ad} can be calculated by two methods. The first refers to unrelaxed supercells. We calculated the total energies of a series of unrelaxed interfaces with different interfacial separation d to get the work of adhesion. The adhesion curves of Al-terminated and Ni-terminated surfaces (shown

in Figure 2) and the W_{ad} with the corresponding interfacial separation d_0 (unrelaxed values) can be obtained. The second refers to the relaxed geometries. We relaxed the interface models with the optimal d_0 and got the work of adhesion, as well as the equilibrium separation d_{eq} (relaxed values). The optimal d_0 and W_{ad} for all unrelaxed and relaxed interface supercells are listed in Table 5. It shows that the work of adhesion of AlNiV (5.01 J/m²) is larger than NiAlV (4.09 J/m²), which is similar to the NiAl/Cr interface [62]. This result supports the previous argument that the surface possessing larger surface energy is more reactive and thus bonding readily. For the interface, the interfacial separations d_{eq} suggests the degree of bond strength. The calculated interfacial separation of the Ni-terminated surface is 1.506 Å shorter than the Al-terminated one, also suggesting that NiAl/V prefers to be Ni-terminated.

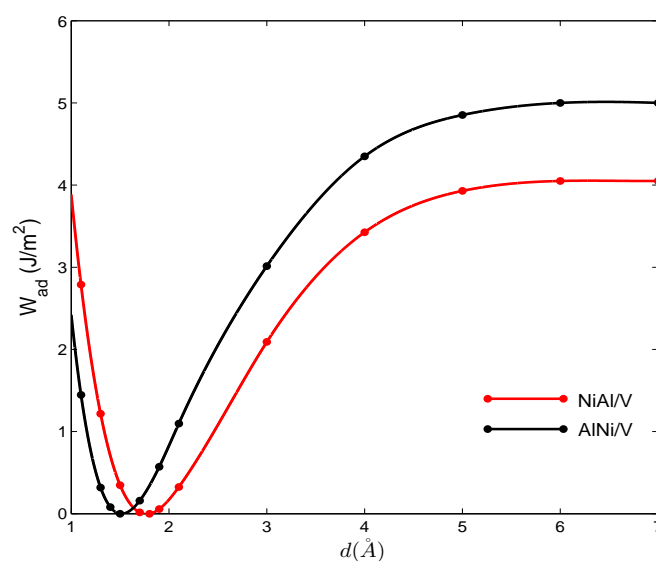


Figure 2. The work of adhesion of the NiAlV and AlNiV interface systems.

Table 5. Interfacial distance d_0 (Å), work of adhesion W_{ad} (J/m²) and interface energy E_{int} (J/m²) using two different methods.

Interfaces	Unrelaxed			Relaxed		
	d_0	W_{ad}	E_{int}	d_{eq}	W_{ad}	E_{int}
NiAlV	1.769	4.09	0.96 ~ 2.30	1.775	4.03	1.02 ~ 2.36
AlNiV	1.515	5.01	0.60 ~ 1.93	1.506	4.85	0.76 ~ 2.09

5.3. Interface Energy

The other one is interface energy E_{int} , which measures the thermal stability of composites. The smaller the interface energy is, the more stable the interfacial geometry is. The interface energy can be viewed as the work required per unit area creating the interface from bulk materials. Generally, it is determined by the following equation [63]:

$$E_{int} = (\gamma_{sA} + \gamma_{sB} - W_{ad}) \quad (6)$$

γ_{sA} and γ_{sB} denote the surface energy of NiAl and V, respectively. According to Equation (6), the interface energy is only related to the surface energy of the Ni-terminated (Al-terminated) surface

and the surface energy of V. However, the surface energy of NiAl with even layers contains the contribution of Ni-terminated and Al-terminated surfaces. The surface energy of Ni-terminated or Al-terminated surfaces must be calculated by using Equation (2). The surface energy of V is calculated using Equation (1) in which the V slab with odd or even layers is always symmetric. The calculated interface energy of AlNiV is 0.76~2.09 J/m² smaller than NiAlV (1.02~2.36 J/m²). Thus, from the thermodynamic view, the AlNiV (Ni-terminated) is more stable.

5.4. Electronic Characteristics

In order to state the details of the interfaces, the difference of the charge density is used to examine the interfacial electronic structure and bonding. The difference of the charge density can be given by the following equation:

$$\Delta\rho = \rho_{A/B} - \rho_A - \rho_B \quad (7)$$

$\rho_{A/B}$ is the total charge density of the interface system; ρ_A and ρ_B are the isolated NiAl and isolated V slabs of the same supercell, respectively. The difference of the charge density of the NiAlV and AlNiV interface systems are presented in Figure 3, respectively. The electron charge rearrangements in the two cases are restricted to one or two layers of the interfaces, demonstrating the importance of the local environment to NiAl-V adhesion. The continuous band of charge accumulation is the characteristic of metallic bonding. The charge reduction in the first metal layer and accumulation at the interface suggest the forming of new bonding with the NiAl layer. Thus, the higher work of adhesion of the Ni-terminated interface is a consequence of a larger contribution of metal-metal bonding at the interface, as reflected in the behavior of the local density of states and the electron density (see below).

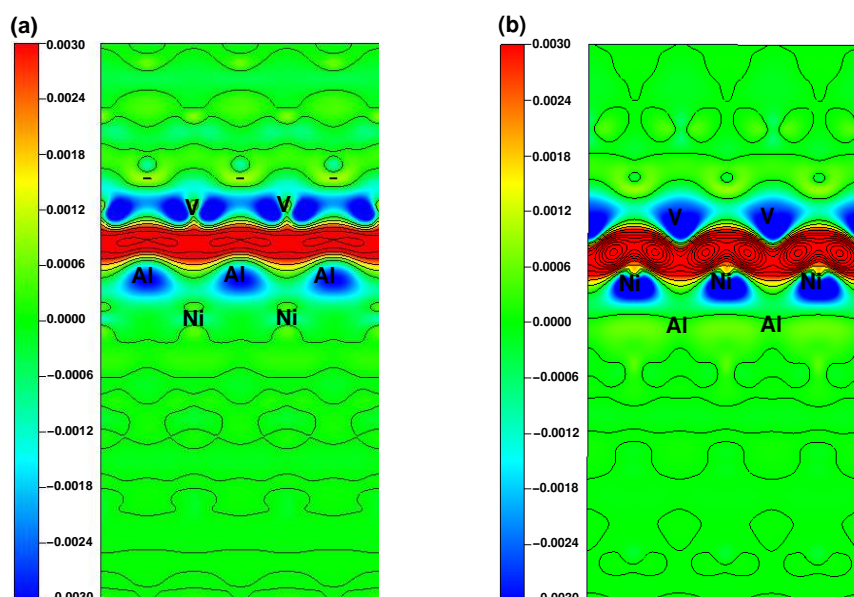


Figure 3. Charge density difference for (a) NiAlV and (b) AlNiV interfaces.

To further reveal the interfacial bonding characteristics, the calculated Layer-Projected Density of States (LPDOS) of the NiAl/V interface with Ni-terminated and Al-terminated surfaces are presented in Figure 4. It is found that the two interface systems have some common features: the effect of the interface on NiAl's and V's DOS is localized and confined to the first layers at two sides near the interface, which is in accordance with the analysis of the difference of the charge density. For the Al-terminated interface, the metallic bonding can be observed through the peak of V's DOS near the

Fermi level. It is found that the shape of the DOS of the interfacial Al and V atoms near the Fermi energy is similar. These overlapping states contribute to hybridization of the V and Al orbital to form covalent bonding. Thus, it is concluded that the interfacial bonding is mixing metallic with covalent. For the Ni-terminated interface, the DOS of the interfacial Ni and V atoms exhibits more occupied states near the Fermi level. The main peak of V's DOS exhibits around 2.5 eV, while the Ni has no new states to overlap. Therefore, the bonding is mainly metallic. The NiAl/V (001) interface has a mismatch, and the metallic interface of Ni-terminated can accommodate more distortions than the Al-terminated interface. Therefore, the Ni-terminated interface is more stable and has larger adhesion, consistent with the previous results.

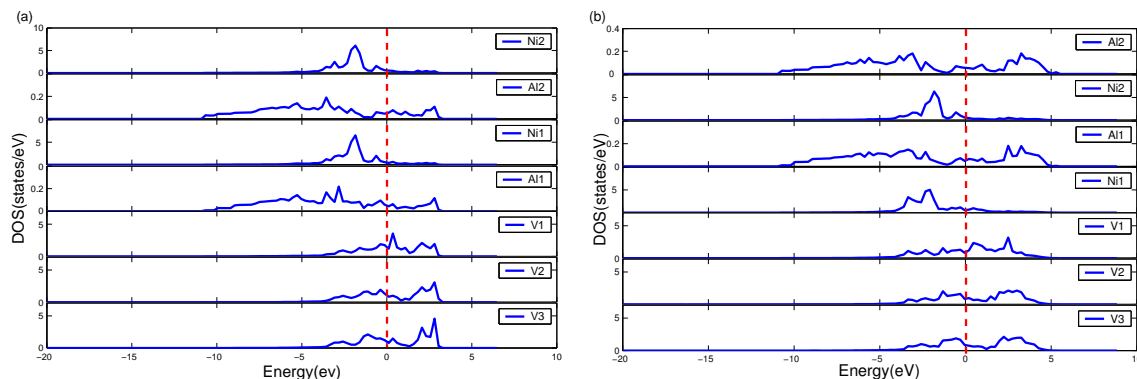


Figure 4. Layer-Projected Density of States (LPDOS) for (a) NiAlV and (b) AlNiV interfaces. The vertical dotted line gives the location of the Fermi level.

6. Semicoherent Interfaces

As we know, there is a discrepancy of the lattice constants between NiAl and V, and the misfit is 4.2%. The misfit will introduce strain energy (stretching V to match NiAl), and the misfit dislocations will be generated to release the strain energy. Therefore, the coherent interfaces become semicoherent interfaces. It is significant to investigate the relative properties of semicoherent interfaces.

6.1. Generalized Stacking Fault Energy of the NiAlV and AlNiV Interfaces

To analyze the dislocation core structure, it is necessary to calculate the Generalized-Stacking-Fault-Energy (GSFE). We calculated the GSFE along $\langle 100 \rangle$ and $\langle 110 \rangle$ in the (001) interface plane with the supercell approach, and the supercells are based on the optimized unit cell. The generalized stacking fault energy is associated with a rigid slip of the upper part of the supercell relative to its lower, fixed part. It can be calculated by:

$$\gamma_{SF}(u) = \frac{E(u) - E(0)}{2A} \quad (8)$$

where u is the slip vector, $E(u)$ and $E(0)$ are the energies of the supercell with and without the stacking fault, respectively, and A is the corresponding stacking fault plane area. The corresponding restoring stress $F(u)$ is considered as the gradient of the generalized stacking fault energy, that is $F(u) = -\frac{\partial \gamma}{\partial u}$ [64–66]. The calculated dependence of the $\gamma_{SF}(u)$ and the restoring force $F(u)$ on the slip displacement u for the Al-terminated and Ni-terminated surfaces are shown in Figure 5. We assume the dislocation core to be confined within the interface plane, and the Burgers vector b is considered to be parallel to the x axis. The maximum values of GSFE is the so-called unstable stacking fault energy γ_{us} , a physical quantity strongly affecting the dislocation core structure. We found that the γ_{us} of the Al-terminated surface is smaller than the Ni-terminated one, which means the NiAlV has lower resistance to shear. This also indicates that weaker bonding between V and Al atoms leads to a lower adhesion energy, which is consistent with the previous results.

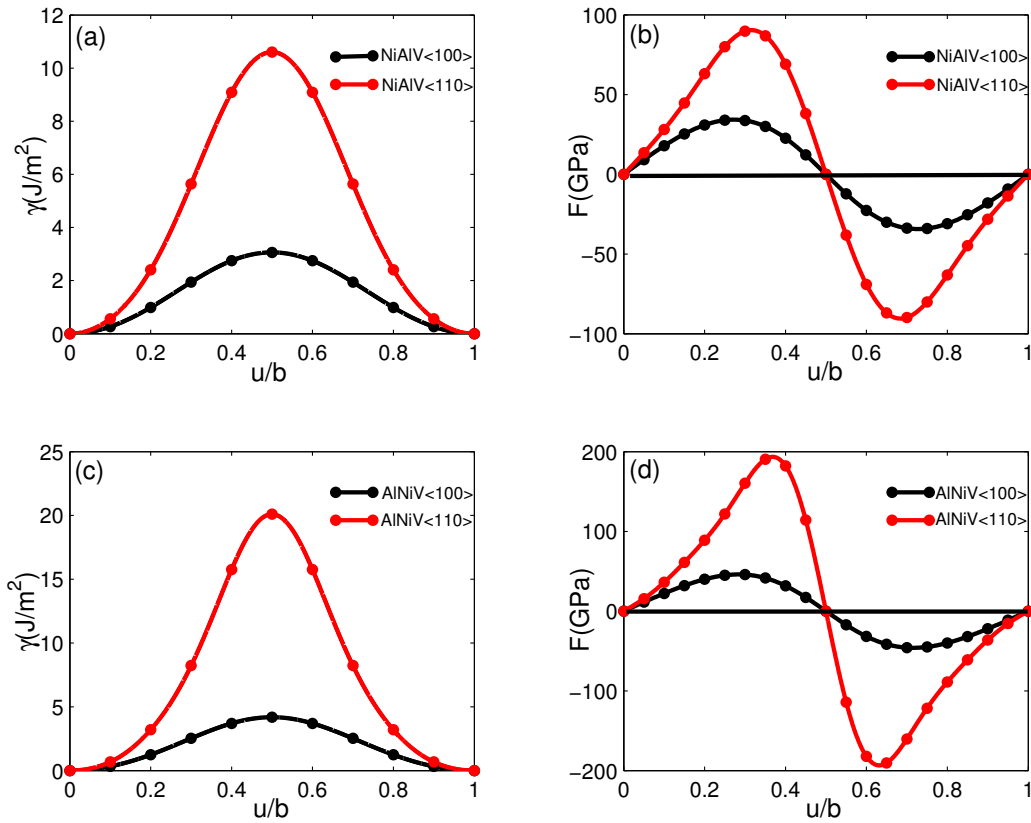


Figure 5. The generalized stacking fault energy curves and the corresponding restoring forces for the NiAlV interface AlNiV interface slip along $\langle 100 \rangle$ and $\langle 110 \rangle$, respectively.

6.2. Core Structure and Energy of Misfit Dislocation

It is difficult to calculate the work of adhesion of semicoherent interfaces through first-principles methods in that the unit cells required for the semicoherent interface are beyond the capacity of our computer. According to Yao *et al.*, the core structure and energy of misfit dislocations at the interfaces can be described using the extended PN theory of misfit dislocations [35,36]. Thus, we performed an approach based on the PN model to estimate the misfit dislocation energy, then employed Equation (6) to figure out the W_{ad} of semicoherent interfaces. In the original work of Yao *et al.*, the PN equation of misfit dislocation is derived as [35]:

$$-\mu \int_{-p/2}^{p/2} \frac{1}{p} \cot\left[\frac{\pi(x-x')}{p}\right] \frac{du(x')}{dx'} dx' = F[U(x)] \quad (9)$$

$p = \frac{a_1 a_2}{a_1 - a_2}$ (a_i is the lattice constant) is defined as the misfit dislocation spacing, and $\mu = \left[\frac{2\mu_2}{\kappa_2 + 1} \right] \left[\frac{1 + \alpha_1}{1 - \alpha_2} \right]$ is relative to the elastic constants of two materials. Here, μ_i is the shear moduli, ν_i is Poisson's ratio ($\kappa_i = 3 - 4\nu_i$) and α_i is the Dundurs parameters [64]. The left-side of Equation (9) is the relevant shear stress along the interface balanced by the corresponding restoring force stress $F(U)$. $U(x)$ is the relative displacement of an atom in the upper part relative to the corresponding atom in the lower part, which contains plastic displacement $u(x)$ and misfit displacement. It can be expressed as:

$$U(x) = \frac{c}{2} + \frac{c}{p}x + u(x) \quad (10)$$

with $c = \frac{2a_1 a_2}{a_1 + a_2}$.

Foreman’s method applied to solve the dislocation equation is given as follows [36]:

$$U(x) = \frac{c}{2} + \frac{c}{\pi} \arctan\left[\frac{1}{a} \tan \frac{\pi x}{p}\right] - f(a) \frac{a^{-2} \tan \frac{\pi x}{p}}{1 + a^{-2} \tan^2\left(\frac{\pi x}{p}\right)} \tag{11}$$

where $f(a) = (\beta - 2a - \beta a^2)/(2a\beta + 2)$ and β can be determined by the maximum of restoring force $F(u)_{max}$ with $\beta = \frac{uf}{F(u)_{max}}$ (the misfit $f = \frac{2(a_1 - a_2)}{(a_1 + a_2)}$). Therefore, the plastic displacement $u(x)$ can be expressed by:

$$u(x) = \frac{c}{\pi} \arctan\left[\frac{1}{a} \tan \frac{\pi x}{p}\right] - f(a) \frac{a^{-2} \tan \frac{\pi x}{p}}{1 + a^{-2} \tan^2\left(\frac{\pi x}{p}\right)} - \frac{c}{p} x \tag{12}$$

Inserting Equation (11) into the left-hand side of Equation (9), the obtained resulting stress is then:

$$F(x) = -\frac{c\mu}{p} \left[\frac{(a^{-2} - 1) \tan\left(\frac{\pi x}{p}\right)}{1 + a^{-2} \tan^2\left(\frac{\pi x}{p}\right)} - f(a) \frac{2a^{-3} \tan\left(\frac{\pi x}{p}\right) + 2a^{-3} \tan^3\left(\frac{\pi x}{p}\right)}{[1 + a^{-2} \tan^2\left(\frac{\pi x}{p}\right)]^2} \right] \tag{13}$$

Let $\theta = \frac{c}{2} + \frac{c}{\pi} \arctan\left[\left(\tan\left(\frac{\pi x}{p}\right)\right)/a\right]$; Equation (11) and Equation (13) can be rewritten as the convenient parametric forms:

$$U(\theta) = \theta + \frac{f(a)c}{2a\pi} \sin\left(\frac{2\pi}{c}\theta\right) \tag{14}$$

$$F(\theta) = -\frac{c\mu}{p} \left[\left(\frac{a}{2} - \frac{1}{2a}\right) \sin\left(\frac{2\pi}{c}\theta\right) + \frac{f(a)}{2} \sin \frac{4\pi}{c}\theta + f(a)(a^{-2} + 1) \sin \frac{2\pi}{c}\theta * \sin^2\left(\frac{\pi}{c}\theta\right) \right] \tag{15}$$

Obviously, we can easily relate the stress $F(U)$ and the displacement U through the parameter θ .

The parameter a can be determined by comparing the shear stress to the restoring force $F(U)$ in that they have the same maximum value. The values of parameter a are presented in Table 6. Therefore, the core structure can be obtained accordingly. It is necessary to know that the parameter a includes the modification of the sinusoidal force law and that β controls the structure of the dislocation. The core structure parameter β is related to the misfit f and the maximum of restoring force $F(u)_{max}$ according to $\beta = \frac{uf}{F(u)_{max}}$. The $F(u)_{max}$ connects to the bond strength τ of the interface according to $F(u)_{max} = \frac{\tau}{2\pi}$ [35]. Thus, the core structure of an interface is influenced by the misfit f and bond strength. The β also suggests that the interface with a higher value of misfit requires a higher bond strength to arrive at the specified dislocation structure. That is, a higher misfit needs a higher coupling across the interface, which was proposed by Vellinga, W.P. *et al.* [67–69]. The misfit dislocation densities $\rho(x) = du(x)/dx$ are plotted in Figure 6 to illustrate the core structure of misfit dislocation, which are found to be very close.

Table 6. The unstable stacking fault energy γ_{us} (J/m²), Burgers vectors b (Å), the misfit dislocation spacing p (Å), parameter a , core structure parameter β , the elastic strain energy E_{ela} (J/m²), misfit energy E_{mis} (J/m²), interface energy E_{int} (J/m²), the work of adhesion W_{ad} (J/m²) for semicoherent and the work of adhesion difference ΔW_{ad} (J/m²) between coherent and semicoherent interfaces.

Misfit Dislocations	γ_{us}	b	p	a	β	E_{ela}	E_{mis}	E_{int}	W_{ad}	$\frac{\Delta W_{ad}}{W_{ad}}$
NiAlV<100>	3.06	2.89	72.5	0.029	0.048	1.83	0.75	2.57	2.48 ~ 3.91	2.4% ~ 38.2%
NiAlV<110>	10.60	4.09	102.5	0.010	0.018	3.63	1.07	4.70	0.36 ~ 1.69	57.8% ~ 91.3%
AlNiV<100>	4.18	2.89	72.5	0.021	0.035	2.06	0.75	2.81	2.80 ~ 4.13	14.5% ~ 41.9%
AlNiV<110>	20.10	4.09	102.5	0.005	0.008	4.43	1.08	5.51	0.10 ~ 1.43	70.3% ~ 97.8%

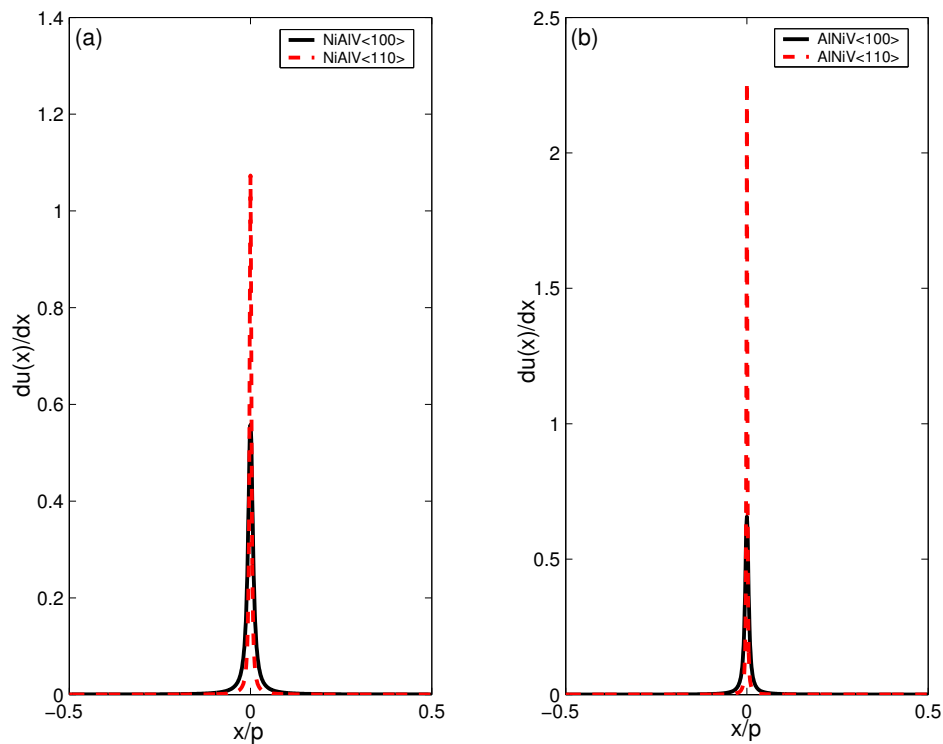


Figure 6. The density of misfit dislocations: (a) NiAlV interface and (b) AlNiV interface for Burgers vector along $\langle 100 \rangle$ and $\langle 110 \rangle$, respectively.

The mean total energy (per unit area) of the interface due to the forming of misfit dislocation is called the interface energy and can be divided into two parts: the elastic strain energy E_{ela} and the misfit energy E_{mis} . The elastic strain energy (per unit area) can be determined by [35]:

$$E_{ela} = -\frac{1}{2p} \int_{-\frac{p}{2}}^{\frac{p}{2}} F(x)u(x)dx \quad (16)$$

The misfit energy (per unit area) can be obtained from:

$$E_{mis} = \frac{1}{p} \int_{-\frac{p}{2}}^{\frac{p}{2}} \Phi[\theta(x)]dx \quad (17)$$

where $\Phi(\theta) = -\int F(\theta)dU(\theta)$. Thus, the mean total interface energy (per unit area) can be expressed as:

$$E = E_{ela} + E_{mis} \quad (18)$$

The calculated elastic strain energy, misfit energy and interface energy are listed in Table 6. Then, the work of adhesion for NiAlV and AlNiV semicoherent interfaces can be calculated by using Equation (6). For the Al-terminated semicoherent interface, the interface energies for misfit dislocations with Burgers vector along $\langle 100 \rangle$ and $\langle 110 \rangle$ are 2.57 J/m² and 4.70 J/m², respectively. Both of them are larger than the coherent interface energy (1.02 ~ 2.36 J/m²). Similarly, the interface energy of AlNiV increases from 0.76 ~ 2.09 J/m² to 2.81 J/m² and 5.51 J/m², respectively. This suggest that the interface energy of the semicoherent interface is larger than that of the coherent interface. Hence, the semicoherent interface posses higher energy than the coherent one, and the work of adhesion will be reduced according to Equation (6). Accordingly, the interfacial adhesion will be reduced. According to the misfit dislocation networks proposed by Trampert *et al.* [70], the obtained results (24.4%) of edge dislocation along the $\langle 100 \rangle$ direction for NiAl/V systems is in the range of the

results (2.4% ~ 41.9%) gained by Forman's method. Our results also coincide well with the previous study [71], which illustrated that the deviation of the W_{ad} due to the exclusion of dislocations may reach 50%. Hence, we can conclude that the misfit dislocations can reduce the interfacial adhesion.

7. Conclusions

The first-principles density functional calculations were employed to investigate the surface properties of NiAl (001) and V (001), as well as the interfacial properties of coherent NiAl/V interfaces. The models of Ni-terminated and Al-terminated surfaces were both considered. The work of adhesion, the interface energy, the difference charge density and the layer-projected density of states were calculated. Furthermore, the semicoherent interfacial properties of NiAl/V interfaces were also investigated within the framework of PN theory for misfit dislocations. The summarized results are given as follows:

(1) Surface tests reveal that the V slab with more than five layers and the NiAl slab with more than seven atomic layers exhibit a bulk-like interior feature, and the surface energy of the Ni-terminated surface is larger than the Al-terminated one for the NiAl slab, which means that the Ni-terminated interface is more active.

(2) The calculated work of adhesion for the Ni-terminated surface (5.01 J/m²) is larger than the Al-terminated one (4.09 J/m²). This means that the NiAl/V systems prefer to be Ni-terminated, in accordance with the analysis of the difference of the charge density and LPDOS. The interface energy of the Ni-terminated surface is smaller than the Al-terminated one, which means the Ni-terminated interface is more stable from a thermodynamic view.

(3) The work of adhesion for both semicoherent Ni-terminated and Al-terminated interfaces is smaller than coherent interfaces. It is found that misfit dislocations can reduce the adhesion of interfaces.

Acknowledgments: The work is supported by the Natural Science Foundation of China (11104361, 11304403, 11547305) and Projects supported by the Fundamental Research Funds for the Central Universities (CDJZR14328801).

Author Contributions: Yaoyao Linghu, Xiaozhi Wu and Rui Wang performed the theoretical calculations; Weiguo Li and Qing Liu analyzed the data; Yaoyao Linghu wrote the paper.

Conflicts of Interest: The authors declare no conflict of interest.

References

1. Baker, I. A review of the mechanical properties of B2 compounds. *Mater. Sci. Eng. A* **1995**, *192*, 1–13.
2. Sivakumar, R.; Mordike, B.L. High temperature coatings for gas turbine blades: A review. *Surf. Coat. Technol.* **1989**, *37*, 139–160.
3. Medvedeva, N.I.; Mryasov, O.N.; Gornostyrev, Y.N.; Novikov, D.L.; Freeman, A.J. First-principles total-energy calculations for planar shear and cleavage decohesion processes in B2-ordered NiAl and FeAl. *Phys. Rev. B* **1996**, *54*, 13506.
4. Grahle, P.; Arzt, E. Microstructural development in dispersion strengthened NiAl produced by mechanical alloying and secondary recrystallization. *Acta Mater.* **1997**, *45*, 201–211.
5. Miracle, D.B. Overview No. 104 The physical and mechanical properties of NiAl. *Acta Metall. Mater.* **1993**, *41*, 649–684.
6. Amouyal, Y.; Rabkin, E.; Mishin, Y. Correlation between grain boundary energy and geometry in Ni-rich NiAl. *Acta Mater.* **2005**, *53*, 3795–3805.
7. Joslin, S.M.; Chen, X.F.; Oliver, B.F.; Noebe, R.D. Fracture behavior of directionally solidified NiAl-Mo and NiAl-V eutectics. *Mater. Sci. Eng. A* **1995**, *196*, 9–18.
8. Hassel, A.W.; Smith, A.J.; Milenkovic, S. Nanostructures from directionally solidified NiAl-W eutectics. *Electrochim. Acta* **2006**, *52*, 1799–1804.
9. Milenkovic, S.; Caram, R. Microstructure of the microalloyed NiAl-V eutectics. *Mater. Lett.* **2002**, *55*, 126–131.

10. Subramanian, P.R.; Mendiratta, M.G.; Miracle, D.B. Microstructures and mechanical behavior of NiAl-Mo and NiAl-Mo-Ti two-phase alloys. *Metall. Mater. Trans. A* **1994**, *25*, 2769–2781.
11. Yang, J.M.; Jeng, S.M.; Bain, K.; Amato, R.A. Microstructure and mechanical behavior of *in-situ* directional solidified NiAl/Cr (Mo) eutectic composite. *Acta Mater.* **1997**, *45*, 295–308.
12. Milenkovic, S.; Coelho, A.A.; Caram, R. Directional solidification processing of eutectic alloys in the Ni-Al-V system. *J. Cryst. Growth* **2000**, *211*, 485–490.
13. Hua, K.; Guo, J.; Ren, Z.; Gao, Q.; Yang, R. Effect of Nb on the microstructure and mechanical properties of cast NiAl-Cr (Mo) eutectic alloy. *J. Mater. Sci. Technol.* **2006**, *22*, 164–168.
14. Cui, C.Y.; Guo, J.T.; Qi, Y.H.; Ye, H.Q. Deformation behavior and microstructure of DS NiAl/Cr (Mo) alloy containing Hf. *Intermetallics* **2002**, *10*, 1001–1009.
15. Whittenberger, J.D.; Noebe, R.D.; Joslin, S.M.; Oliver, B.F. Elevated temperature compressive slow strain rate properties of several directionally solidified NiAl-(Nb,Mo) alloys. *Intermetallics* **1999**, *7*, 627–633.
16. Zeumert, B.; Sauthoff, G. Intermetallic NiAl-Ta alloys with strengthening Laves phase for high-temperature applications. I. Basic properties. *Intermetallics* **1997**, *5*, 563–577.
17. Milenkovic, S.; Caram, R. Mechanical properties and fracture behavior of directionally solidified NiAl-V eutectic composites. *Metall. Mater. Trans. A* **2015**, *46*, 557–565.
18. Choudhury, S.; Agular, J.A.; Fluss, M.J.; Hsiung, L.L.; Misra, A.; Uberuaga, B.P. Non-uniform solute segregation at semi-coherent metal/oxide interfaces. *Sci. Rep.* **2015**, *5*, 13086.
19. Choudhury, S.; Morgan, D.; Uberuaga, B.P. Massive interfacial reconstruction at misfit dislocations in metal/oxide interfaces. *Sci. Rep.* **2014**, *5*, 6533.
20. Benedek, R.; Alavi, A.; Seidman, D.N.; Yang, L.H.; Muller, D.A.; Woodward, C. First principles simulation of a ceramic metal interface with misfit. *Phys. Rev. Lett.* **2000**, *84*, 3362.
21. Lu, S.; Hu, Q.M.; Punkkinen, M.P.J.; Johansson, B.; Vitos, L. First-principles study of fcc-Ag/bcc-Fe interfaces. *Phys. Rev. B* **2013**, *87*, 22104.
22. Benedek, R.; Seidman, D.N.; Minkoff, M.; Yang, L.H.; Alavi, A. Atomic and electronic structure and interatomic potentials at a polar ceramic/metal interface: {222} MgO/Cu. *Phys. Rev. B* **1999**, *60*, 16094.
23. Arya, A.; Carter, E.A. Structure, bonding, and adhesion at the TiC (100)/Fe (110) interface from first principles. *J. Chem. Phys.* **2003**, *118*, 8982–8996.
24. Muñoz, M.C.; Gallego, S.; Beltrán, J.I.; Cerdá, J. Adhesion at metal-ZrO₂ interfaces. *Sur. Sci. Rep.* **2006**, *61*, 303–344.
25. Shang, J.X.; Guan, K.; Wang, F.H. Atomic structure and adhesion of the Nb(001)/ α -Nb₅Si₃(001) interface: A first-principles study. *J. Phys. Condens. Matter* **2010**, *22*, 085004.
26. Jung, J.; Cho, M.; Zhou, M. Ab initio study of the fracture energy of LiFePO₄/FePO₄ interfaces. *J. Power Sources* **2013**, *243*, 706–714.
27. Li, J.; Qi, Y.N.; Zhang, M.; Zhou, Y.; Li, X. First-principle study of adhesion, wetting and bonding on Al/Al₃V (001) interface. *Surf. Sci.* **2014**, *624*, 1–7.
28. Dong, N.; Zhang, C.; Liu, H.; Fan, G.; Fang, X.D.; Han, P. Effects of different alloying additives X (X = Si, Al, V, Ti, Mo, W, Nb, Y) on the adhesive behavior of Fe/Cr₂O₃ interfaces: A first-principles study. *Comput. Mater. Sci.* **2015**, *109*, 293–299.
29. Junkaew, A.; Ham, B.; Zhang, R.X. Arróyave, Investigation of interfaces in Mg/Nb multilayer thin films. *Comput. Mater. Sci.* **2015**, *108*, 212–225.
30. Pan, Y.; Lin, Y.H.; Wang, H.; Guo, J.M.; Singh, A.; Fu, C.Y. Interfacial stability, electronic structure and bond characteristics of Pt₃Zr(111)/Pt (111) interfaces: A first-principles study. *Comput. Mater. Sci.* **2016**, *111*, 74–78.
31. Wang, Y.; Liu, Z.-K.; Chen, L.-Q.; Wolverton, C. First-principles calculations of β'' -Mg₅Si₆/ α -Al interfaces. *Acta Mater.* **2007**, *55*, 5934–5937.
32. Finns, M.W. The theory of metal-ceramic interfaces. *J. Phys. Condens. Matter* **1996**, *8*, 5811–5836.
33. Joos, B.; Duesbery, M.S. The Peierls stress of dislocations: An analytic formula. *Phys. Rev. Lett.* **1997**, *78*, 266.
34. Schoeck, G. The core structure, recombination energy and Peierls energy for dislocations in Al. *Philos. Mag. A* **2001**, *81*, 1161–1176.
35. Yao, Y.; Wang, T.C.; Wang, C.Y. Peierls-Nabarro model of interfacial misfit dislocation: An analytic solution. *Phys. Rev. B* **1999**, *59*, 8232.

36. Yao, Y.; Wang, T.C. The modified Peierls-Nabarro model of interfacial misfit dislocation. *Acta Mater.* **1999**, *47*, 3063–3068.
37. Zhang, Y.; Yao, Y. The two-dimensional Peierls-Nabarro model for interfacial misfit dislocation networks of cubic lattice. *Eur. Phys. J. B* **2007**, *55*, 355–362.
38. Zhang, Y.; Yao, Y. The multiscale model combining elastic theory with ab initio calculations for metal-ceramic interfaces. *Mod. Phys. Lett. B* **2008**, *22*, 3135–3143.
39. Johansson, S.A.E.; Christensen, M.; Wahnstrom, G. Interface energy of semicoherent metal-ceramic interfaces. *Phys. Rev. Lett.* **2005**, *95*, 226108.
40. Fors, D.H.R.; Johansson, S.A.E.; Petisme, M.V.G.; Wahnstrom, G. Theoretical investigation of moderate misfit and interface energetics in the Fe/VN system. *Comput. Mater. Sci.* **2010**, *50*, 550–559.
41. Medvedeva, N.I.; Gornostyrev, Y.N.; Kontsevoi, O.Y.; Freeman, A.J. Ab-initio study of interfacial strength and misfit dislocations in eutectic composites: NiAl/Mo. *Acta Mater.* **2004**, *52*, 675–682.
42. Kresse, G.; Hafner, J. Ab initio molecular dynamics for liquid metals. *Phys. Rev. B* **1993**, *47*, 558.
43. Kresse, G.; Furthmüller, J.; Hafner, J. Ab initio force constant approach to phonon dispersion relations of diamond and graphite. *Phys. Rev. B* **1995**, *32*, 729.
44. Blöchl, P.E. Projector augmented-wave method. *Phys. Rev. B* **1994**, *50*, 17953.
45. Kresse, G.; Joubert, D. From ultrasoft pseudopotentials to the projector augmented-wave method. *Phys. Rev. B* **1999**, *59*, 1758.
46. Perdew, J.P.; Burke, K.; Ernzerhof, M. Generalized gradient approximation made simple. *Phys. Rev. Lett.* **1996**, *77*, 3865.
47. Lazar, P.; Podloucky, R. Ab initio study of the mechanical properties of NiAl microalloyed by X= Cr, Mo, Ti, Ga. *Phys. Rev. B* **2006**, *73*, 104114.
48. Ponomareva, A.V.; Isaev, E.I.; Vekilov, Y.K.; Abrikosov, I.A. Site preference and effect of alloying on elastic properties of ternary B2 NiAl-based alloys. *Phys. Rev. B* **2012**, *85*, 144117.
49. Rai, R.C.; Hemkar, M.P. Crystal equilibrium and lattice dynamics of chromium and vanadium. *J. Phys. F Met. Phys.* **1978**, *8*, 45.
50. Bolef, D.I. Elastic constants of single crystals of the bcc transition elements V, Nb, and Ta. *J. Appl. Phys.* **1961**, *32*, 100.
51. Born, M.; Huang, K. *Dynamical Theory of Crystal Lattices*; Oxford University Press: Oxford, UK, 1998.
52. Hill, R. The elastic behaviour of a crystalline aggregate. *Proc. Phys. Soc. A* **1952**, *65*, 349.
53. Ravindran, P.; Fast, L.; Korzhavyi, P.A.; Johansson, B. Density functional theory for calculation of elastic properties of orthorhombic crystals: Application to TiSi₂. *J. Appl. Phys.* **1998**, *84*, 4891–4904.
54. Liu, W.; Li, J.C.; Zheng, W.T.; Jiang, Q. NiAl(110)/Cr(110) interface: A density functional theory study. *Phys. Rev. B* **2006**, *73*, 205421.
55. Fiorentini, V.; Methfessel, M. Extracting convergent surface energies from slab calculations. *J. Phys. Condens. Matter* **1996**, *8*, 6525.
56. Zhang, J.M.; Ma, F.; Xu, K.W. Calculation of the surface energy of bcc metals by using the modified embedded-atom method. *Surf. Interface Anal.* **2003**, *34*, 662–666.
57. Neugebauer, J.; Scheffler, M. Adsorbate-substrate and adsorbate-adsorbate interactions of Na and K adlayers on Al (111). *Phys. Rev. B* **1992**, *46*, 16067.
58. Liu, L.M.; Wang, S.Q.; Ye, H.Q. First-principles study of polar Al/TiN (111) interfaces. *Acta Mater* **2004**, *52*, 3681–3688.
59. Siegel, D.J.; Hector, L.G.; Adams, J.B. Adhesion, atomic structure, and bonding at the Al(111)/ α -Al₂O₃ (0001) interface: A first principles study. *Phys. Rev. B* **2002**, *65*, 085415.
60. Brown, J.A.; Mishin, Y. Monte Carlo modeling of low-index surfaces in stoichiometric and Ni-rich NiAl. *Phys. Rev. B* **2003**, *67*, 195414.
61. Kriese, M.D.; Moody, N.R.; Gerberich, W.W. Effects of annealing and interlayers on the adhesion energy of copper thin films to SiO₂/Si substrates. *Acta Mater.* **1998**, *46*, 6623–6630.
62. Reynolds, J.E.; Smith, J.R.; Zhao, G.L.; Srolovitz, D.J. Adhesion in NiAl-Cr from first principles. *Phys. Rev. B* **1996**, *53*, 13883.
63. Christensen, M.; Dudiy, S.; Wahnström, G. First-principles simulations of metal-ceramic interface adhesion: Co/WC versus Co/TiC. *Phys. Rev. B* **2002**, *65*, 045408.
64. Suo, Z.; Hutchinson, J.W. Interface crack between two elastic layers. *Int. J. Fract.* **1990**, *43*, 1–18.

65. Vitek, V. Intrinsic stacking faults in body-centred cubic crystals. *Philos. Mag.* **1968**, *18*, 773–786.
66. Wang, C.; Wang, C.Y. Density functional theory study of Ni/Ni₃Al interface alloying with Re and Ru. *Surf. Sci.* **2008**, *602*, 2604–2609.
67. De Hosson, J.T.M.; Groen, H.B.; Kooi, B.J.; Vitek, V. Metal-ceramic interfaces studied with high-resolution transmission electron microscopy. *Acta Mater.* **1999**, *47*, 4077–4092.
68. Vellinga, W.P.; De Hosson, J.T.M.; Vitek, V. Misfit dislocations: An atomistic and elastic continuum approach. *Acta Mater.* **1997**, *45*, 1525–1534.
69. Vellinga, W.P.; De Hosson, J.T.M. Atomic structure and orientation relation of interfaces between Ag and ZnO. *Acta Mater.* **1997**, *45*, 933–950.
70. Trampert, A.; Ernst, F.; Flynn, C.P.; Fischmeister, H.F.; Ruhle, M. High resolution transmission electron microscopy studies of the Ag/MgO interface. *Acta Metall. Mater.* **1992**, *40*, S227–S236.
71. Schnitker, J.; Srolovitz, D.J. Misfit effects in adhesion calculations. *Model. Simul. Mater. Eng.* **1998**, *6*, 153–164.



© 2016 by the authors; licensee MDPI, Basel, Switzerland. This article is an open access article distributed under the terms and conditions of the Creative Commons by Attribution (CC-BY) license (<http://creativecommons.org/licenses/by/4.0/>).